1　　**Reversal of β-amyloid induced microglial toxicity *in vitro* by activation of Fpr2/3**

2

3　　Edward S. Wickstead[1,2], Husnain A. Karim[1], Roberta E. Manuel[1], Christopher Biggs[2], Stephen

4　　J. Getting[2] & Simon McArthur[1,*]

5

6　　[1.]Institute of Dentistry, Barts & the London School of Medicine & Dentistry, Queen Mary,

7　　University of London, Blizard Institute, 4, Newark Street, London, E1 2AT, UK

8　　[2.] College of Liberal Arts & Sciences, University of Westminster, 115, New Cavendish Street,

9　　London W1W 6UW, UK

10

11　　* Correspondence to Dr Simon McArthur, s.mcarthur@qmul.ac.uk

12

13

14

15

16

17

18   **Abstract**

19

20   **Background and Purpose**

21   Microglial inflammatory activity is thought to be a major contributor to the pathology of
22   neurodegenerative conditions such as Alzheimer's disease (AD), and strategies to restrain
23   their behaviour are under active investigation. Classically, anti-inflammatory approaches aim
24   to suppress pro-inflammatory mediator production, but exploitation of inflammatory resolution,
25   the endogenous process whereby an inflammatory reaction is terminated, has not been fully
26   investigated as a therapeutic approach in AD. In this study, we sought to provide proof-of-
27   principal that the major pro-resolving actor, formyl peptide receptor 2, Fpr2, could be targeted
28   to reverse microglial activation induced by the AD-associated pro-inflammatory stimulus,
29   oligomeric β-amyloid (oAβ).

30

31   **Experimental Approach**

32   The immortalised murine microglial cell line BV2 was employed as a model system to
33   investigate the pro-resolving effects of the Fpr2 ligand QC1 upon oAβ-induced inflammatory,
34   oxidative and metabolic behaviour. Cytotoxic behaviour of BV2 cells was assessed through
35   use of co-cultures with retinoic acid-differentiated human SH-SY5Y cells.

36

37   **Key Results**

38   Stimulation of BV2 cells with oAβ at 100nM did not induce classical inflammatory marker
39   production but did stimulate production of reactive oxygen species (ROS), an effect that could
40   be reversed by subsequent treatment with the Fpr2 ligand QC1. Further investigation revealed
41   that oAβ-induced ROS production was associated with NADPH oxidase activation and a shift
42   in BV2 cell metabolic phenotype, activating the pentose phosphate pathway and NADPH
43   production, changes that were again reversed by QC1 treatment. Microglial oAβ-stimulated
44   ROS production was sufficient to induce apoptosis of bystander SH-SY5Y cells, an effect that
45   could be prevented by QC1 treatment.

46

47   **Conclusion and Implications**

48   In this study, we provide proof-of-concept data that indicate exploitation of the pro-resolving
49   receptor Fpr2 can reverse damaging oAβ-induced microglial activation. Future strategies
50   aiming to restrain neuroinflammation in conditions such as AD should examine pro-resolving
51   actors as a mechanism to harness the brain's endogenous healing pathways and limit
52   neuroinflammatory damage.

53

54   **Keywords**: Fpr2/3, Microglia, Oxidative stress, Alzheimer's disease

Background

AD is the single greatest cause of dementia, affecting approximately 4% of individuals aged over 65 years and with a global disease burden of around 37 million individuals [1]. This figure is set to increase as the population ages, and is expected to reach around 78 million people by 2050 [2]. There are currently no effective treatments for the condition.

Whilst the two core pathological lesions of AD, extracellular β-amyloid (Aβ) plaques and intraneuronal tau tangles, have long been studied, the contribution to pathology provided by neuroinflammation, and the role of the microglia in AD pathogenesis, has only recently been appreciated [3,4]. Several lines of evidence indicate a pathological role for microglial activity: studies of genetic risk factors for idiopathic AD have identified numerous immune-related risk loci, clinical imaging studies indicate a positive correlation between microglial activity and both Aβ load and neurodegeneration [5], and chronic neuroinflammation is a feature of multiple independent animal models of the disease [6]. More directly, Aβ can act as a damage-associated molecular pattern [7], stimulating microglial activation through a range of different receptors, including the receptor for advanced glycation end products, toll-like receptors, and CD36 [8].

Under normal conditions, inflammation is self-resolving, with numerous factors acting to 'switch off' inflammatory processes [9]. A central actor in this process is the G protein-coupled receptor formyl peptide receptor 2 (FPR2) or its murine functional homologues Fpr2/3 [10]. Strong evidence exists for the pro-resolving potential of this receptor in peripheral inflammation, where it promotes neutrophil apoptosis [11], and regulates monocyte/macrophage recruitment [12,13], phenotype [14] and behaviour [15]. Importantly, protective effects have been identified for this receptor in diverse inflammatory settings, including sepsis [16], heart failure [17] and atherosclerosis [18].

Expression of FPR2 within the brain has been reported in the endothelium and in selected hippocampal and cerebellar neurones [19], but it is also expressed by microglia [20], and is rapidly upregulated following inflammatory insult [21]. Significantly, FPR2 expression has been reported in inflammatory cells infiltrating Aβ plaques in AD [22], is involved in chemotaxis to high concentrations of Aβ [23] and has been indirectly implicated in microglial Aβ phagocytosis [24]. Given the importance of this receptor in the resolution of peripheral inflammation, we hypothesised that FPR2 agonists would be able to reverse the pro-inflammatory effects of Aβ upon microglia, restoring normal homeostasis.

92   **Methods**

93

94   *Drugs & Reagents*

95   The FPR2 agonist Quin-C1 (QC1; 4-Butoxy-N-[1,4-dihydro-2-(4-methoxyphenyl)-4-oxo-
96   3(2H)-quinazolinyl]benzamide) and antagonist WRW_4 (Trp-Arg-Trp-Trp-Trp-Trp-NH_2) were
97   purchased from Tocris Ltd, UK. Isolated and purified lipopolysaccharides developed in
98   *Escherichia* coli, serotype O111:B4 were purchased from Perck Millipore, Ltd, UK. HFIP-
99   treated human $A\beta_{1-42}$ peptide was purchased from JPT Peptide Technologies, Berlin,
100   Germany.

101

102   *Aβ oligomerisation*

103   HFIP-treated $A\beta_{1-42}$ stored at -80°C in DMSO was oligomerised by dilution and vortexing in
104   PBS followed by incubation overnight at 4°C [25]. Oligomer formation was confirmed by native
105   Tricine-SDS-polyacrylamide gel electrophoresis. Briefly, 2 µg oligomeric Aβ (oAβ) was
106   resuspended in non-denaturing sample buffer (62.5 mM Tris-base, 25% glycerol, 1% (w/v)
107   Coomassie Blue R-250) and loaded onto a 10% acrylamide:bis-acrylamide gel and separated
108   by electrophoresis alongside molecular weight markers. Gels were incubated with Coomassie
109   stain (60mg/l Coomassie Blue R-250, 10% v/v acetic acid, both Sigma, UK) Following 24h de-
110   staining in 10% v/v acetic acid, 50% v/v methanol (Sigma, UK), gels were imaged using a
111   ChemiDoc MP Imaging System (Bio-Rad Ltd., UK). Oligomeric Aβ migrated at approximately
112   35kDa, indicating the presence of hexamers/heptamers (Supplemental Figure 1).

113

114   *Cell culture*

115   The murine microglial line BV2 were a generous gift from Prof. E. Blasi (Università degli Studi
116   di Modena e Reggio Emilia, Italy); the human neuroblastoma SH-SY5Y line was purchased
117   from the European Collection of Authenticated Cell Cultures (ECACC, Salisbury, UK). Both
118   lines were cultured in DMEM medium supplemented with 5% fetal calf serum and 100 µM
119   non-essential amino acids, 2 mM L-alanyl-L-glutamine and 50 mg/ml penicillin-streptomycin
120   (all Thermofisher Scientific, UK) at 37°C in a 5% CO_2 atmosphere. SH-SY5Y cells were
121   differentiated to a neurone-like phenotype prior to experimentation by incubation with 10 µM
122   trans-retinoic acid (Sigma, UK) for 5 days [26].

123

124   *Reactive oxygen species (ROS) assays*

125   Total intracellular ROS production was quantified using 6-chloromethyl-2',7'-
126   dichlorodihydrofluorescein diacetate, acetyl ester (CM-H_2DCFDA; Thermofisher Scientific,
127   UK) according to the manufacturer's recommendations. Briefly, cells were plated at 200,000
128   cells/cm^2 in phenol red-free DMEM, serum starved overnight and pre-loaded with 5 µM CM-

129   H$_2$DCFDA for 20 minutes at 37°C. Following removal of unbound dye, fresh phenol red free-

130   DMEM was added and experimental treatments were begun. Following administration of

131   treatments, cellular fluorescence was determined every 5 minutes for 1 hr at 37°C using a

132   CLARIOstar fluorescence microplate reader (BMG Labtech, Germany) with excitation and

133   emission filters set at 492nm and 517nm respectively.

134

135   Mitochondrial superoxide production was quantified using the tracer MitoSOX Red

136   (Thermofisher Scientific, UK) according to the manufacturer's recommendations and a loading

137   concentration of 2.5 μM. Following administration of treatments, cellular fluorescence was

138   determined every 5 minutes for 1 hr at 37°C using a CLARIOstar fluorescence microplate

139   reader (BMG Labtech, Germany) with excitation and emission filters set at 510nm and 580nm

140   respectively.

141

142   Hydrogen peroxide production was quantified using the ROS-Glo H$_2$O$_2$ assay (Promega,

143   Southampton, UK) according to the manufacturer's recommendations. Following experimental

144   treatment, luminescence of cell lysates at 37°C was determined using a CLARIOstar

145   luminescence microplate reader (BMG Labtech, Germany), in comparison to a H$_2$O$_2$ standard

146   curve (0.013 μM – 10 mM).

147

148   *GSH:GSSG ratio analysis*

149   The ratio of reduced (GSH) to oxidised (GSSG) glutathione was determined using a

150   commercial assay (GSH:GSSG-Glo assay, Promega Co, Southampton, UK) according to the

151   manufacturer's instructions, with cells plated at 200,000 cells/cm^2 on black walled 96-well

152   plates. A CLARIOstar spectrophotometer (BMG Labtech, Germany) was used to measure

153   relative luminescence with comparison to a total glutathione standard curve (0.25 μM – 16

154   μM).

155

156   *Cytokine ELISA*

157   Tumour necrosis factor alpha (TNFα), was assayed by murine-specific sandwich ELISA using

158   commercially available kits, according to the manufacturer's protocols (ThermoFisher

159   Scientific, UK). A CLARIOstar spectrophotometer (BMG Labtech, Germany) was used to

160   measure absorbance at 450 nm.

161

162   *E. coli bioparticle phagocytosis*

163   Microglial phagocytic capacity was determined using BODIPY-FL conjugated *Escherichia coli*

164   (K-12 strain) bioparticles (ThermoFisher Scientific, UK). Following experimental treatments,

165   cells were incubated with bioparticle conjugates at a ratio of 50 particles per cell in PBS for 30

166   minutes at 37°C in the dark. Cells were washed, fluorescence of non-engulfed particles was

167   quenched by addition of 0.2% Trypan blue (ThermoFisher Scientific, UK) for 1 min, and cellular

168   fluorescence was determined using a FACS Canto II flow cytometer (BD Biosciences, UK)

169   equipped with a 488nm laser and FlowJo 8.8.1 software (Treestar Inc. FL, USA). A total of

170   10,000 singlet events per sample were quantified.

171

172   *Flow cytometry*

173   BV2 or SH-SY5Y cells alone or in co-culture were labelled with APC-conjugated rat

174   monoclonal anti-mouse CD11b, PE-Cy7-conjugated rat monoclonal anti-mouse CD40

175   (Biolegend, UK) or PerCP-Cy5.5-conjugated mouse monoclonal anti-human CD200 (all

176   Biolegend, UK) for analysis by flow cytometry. Immunofluorescence was analysed for 10,000

177   singlet events per sample using a BD FACSCanto II (BD Biosciences, UK) flow cytometer;

178   data were analysed using FlowJo 8.8.1 software (Treestar Inc., CA, USA).

179

180   *Annexin A5 apoptosis assay*

181   SH-SY5Y cells were differentiated as described above and treated according to experimental

182   design, either alone or in co-culture with BV2 cells. cultures were in PBS, detached using a

183   cell scraper and incubated with FITC-conjugated annexin A5 (0.45 µg/ml in 0.01 M PBS, 0.1%

184   bovine serum albumin, 1 mM $CaCl_2$), and in the case of co-cultures, APC-conjugated rat

185   monoclonal anti-mouse CD11b and PerCP-Cy5.5-conjugated mouse monoclonal anti-human

186   CD200 (all Biolegend, UK) on ice in the dark for 30 min. Samples were washed and analysed

187   by flow cytometry. Immunofluorescence was analysed for 10,000 singlet events per sample

188   using a BD FACSCanto II (BD Biosciences, UK) flow cytometer; data were analysed using

189   FlowJo 8.8.1 software (Treestar Inc., CA, USA).

190

191   *Western blot analysis*

192   Samples boiled in 6× Laemmli buffer were subjected to standard SDS-PAGE (10%) and

193   electrophoretically blotted onto Immobilon-P polyvinylidene difluoride membranes (Merck,

194   UK). Total protein was quantified using Ponceau S staining (Merck, UK) and membranes were

195   blotted using antibodies raised against murine haem oxygenase-1 (HO-1; rabbit polyclonal,

196   1:1000, Cell Signaling Technology, Leiden, The Netherlands) or superoxide dismutase 2

197   (SOD2; rabbit monoclonal, 1:1000, Cell Signaling Technology, Leiden, The Netherlands) in

198   Tris-buffer saline solution containing 0.1% Tween-20 and 5% (w/v) non-fat dry milk overnight

199   at 4ºC. Membranes were washed with Tris-buffer saline solution containing 0.1% Tween-20,

200   and incubated with secondary antibody (horseradish peroxidase–conjugated goat anti-rabbit

201   1:5,000; ThermoFisher Scientific, UK), for 90 min at room temperature. Proteins were then

202   detected using enhanced chemiluminescence detection (2.5 mM luminol, 0.4 mM p-coumaric

203   acid, 7.56 mM H_2O_2 in 1 M Tris, pH 8.5) and visualised on X-ray film (Scientific Laboratory

204   Supplies Limited, Nottingham, UK). Films were digitized and analysed using ImageJ 1.51w

205   software (National Institutes of Health).

206

207   *Immunofluorescence & confocal microscopy*

208   Following experimental treatment, BV2 cells cultured in chambered microslides were fixed by

209   incubation in 2% formaldehyde in PBS for 10 min at 4°C, washed and non-specific antibody

210   binding was minimised by incubation for 30 min at room temperature in PBS containing 10%

211   FCS and 0.05% Triton X-100 (all Thermofisher Scientific, UK). Cells were then incubated with

212   rabbit anti-mouse p67Phox monoclonal antibody (1:500, clone EPR5064, Abcam Ltd,

213   Cambridge, UK) and mouse anti-mouse gp91phox monoclonal antibody (1:50, clone 53, BD

214   Biosciences, UK) overnight at 4°C in PBS with 1% FCS and 0.05% Triton X-100. Cells were

215   washed and incubated with AF488-conjugated goat anti-mouse and AF647-conjugated goat

216   anti-rabbit secondary antibodies (both 1:500, Thermofisher Scientific, UK) in PBS with 1%

217   FCS and 0.05% Triton X-100 at room temperature for 1 hr. Cells were washed with PBS,

218   nuclei were defined by incubation with 180 nM DAPI in ddH_2O for 5 min, and cells were

219   mounted under Mowiol mounting solution. Cells were imaged using an LSM710 confocal

220   microscope (Leica, UK) fitted with 405nm, 488nm and 647nm lasers and a 63x oil immersion

221   objective lens (NA 1.4mm, working distance 0.17mm). Images were captured with ZEN Black

222   software (Zeiss, Cambridge, UK) and analysed with ImageJ 1.51w (National Institutes of

223   Health, USA).

224

225   *Glucose 6-phosphate dehydrogenase activity assay*

226   Glucose 6-phosphate dehydrogenase (G6PD) activity was assessed using a commercial

227   assay (Cell Signalling Technology, UK) according to the manufacturer's instructions. Following

228   treatment according to experimental design, cells were lysed by ultrasonication (2 x 20s at

229   20kHz) in assay lysis buffer (22 mM Tris-HCl, 150 mM NaCl, 1 mM Na_2EDTA, 1 mM EGTA,

230   1% Triton X-100, 20 mM sodium pyrophosphate, 25 mM sodium fluoride, 1 mM β-

231   glycerophosphate, 1 mM sodium orthovanadate, 1 µg/ml leupeptin, 1 mM phenylmethane

232   sulfonyl fluoride, pH 7.5, 4°C) using a Soniprep 150 (BMG Labtech, UK), centrifuged at

233   14000g and 4°C for 10 min, and lysates were collected. Samples were diluted to 0.2 mg/ml in

234   assay buffer, incubated at 37°C for 15 min with assay substrate and fluorescence analysed

235   using a CLARIOstar spectrophotometer (BMG Labtech, Germany) with excitation and

236   emission filters set at 540nm and 590nm respectively.

237

238   *Mitochondrial function assay*

239   Mitochondrial function was assessed using a Seahorse XF24 cell MitoStress Test (Agilent

240   Technologies, California, USA) according to the manufacturer's instructions. BV2 cells plated

241   at 2×10^6 cells/cm^2 were serum starved overnight and treated according to experimental

242   design. Medium was replaced with Seahorse XF DMEM supplemented with 1 g/L glucose and

243   1 mM sodium pyruvate, pH 7.4 (Sigma, UK) and cells were incubated at 37°C without CO_2 for

244   45 min prior to analysis of oxygen consumption rate (OCR) and extracellular acidification rate

245   (ECAR). Basal respiration was initially determined prior to subsequent serial cellular

246   treatments with 4 µM oligomycin, 0.6 µM FCCP and 1 µM rotenone/antimycin A to measure

247   ATP production, maximal respiratory capacity and non-mitochondrial respiration, respectively.

248   For each treatment, readings were taken in triplicate every 5 min. Cells were lysed in RIPA

249   buffer and protein content was assessed by Bradford's method for sample normalisation.

250   Rates of glycolytic and oxidative ATP production were then calculated as described in [27].

251

252   *Statistical analysis*

253   Sample sizes were calculated to detect differences of 15% or more with a power of 0.85 and

254   α set at 5%, calculations being informed by previously published data [28,29]. All experimental

255   data are presented as mean ± SEM, repeated using a minimum of n = 3 independent culture

256   flasks; assays were performed in triplicate. In all cases, normality of distribution was

257   established using the Shapiro–Wilk test, followed by analysis with two-tailed Student's t tests

258   to compare two groups or, for multiple comparison analysis, one- or two-way ANOVA followed

259   by Tukey's HSD *post hoc* test, a $p < 0.05$ was considered statistically significant. All statistical

260   analysis was performed using Graph Pad Prism 8 software (GraphPad Software, CA, USA).

261

262   **Results**

263

264   *AD-relevant concentrations of Aβ do not induce an inflammatory response in BV2 microglia*

265   Whilst many studies have investigated the toxic properties of Aβ, these have in general used

266   micromolar concentrations of the peptide, levels which are unlikely to be achieved until the

267   end stages of AD [30]. We sought to determine the potential of Fpr2/3 as a target to control

268   Aβ-driven inflammation earlier in the disease process when oligomeric Aβ is found in the

269   nanomolar range [30], hence we characterised the inflammatory response of BV2 cells to AD-

270   relevant concentrations of Aβ. Initial studies identified a clear dose-dependent increase in BV2

271   cell reactive oxygen species (ROS) production upon Aβ stimulation (Figure 1A), with 100 nM

272   Aβ stimulating an approximately 2.5 fold increase; this concentration of Aβ was thus used for

273   further investigation.

274

275   In contrast to ROS production however, 100 nM Aβ did not elicit other inflammatory changes

276   in BV2 cells, whether assessed through production of the major inflammatory cytokine TNFα

277   (Figure 1B), induction of the inflammatory surface phenotypic marker CD40 (Figure 1C) or

278   phagocytosis of labelled *E. coli* bioparticles (Figure 1D). This was in marked contrast to the

279   effects of bacterial lipopolysaccharide (LPS) which was able to evoke a clear inflammatory

280   response from BV2 cells (Figure 1B-D).

281

282   *oAβ induces ROS production through NADPH oxidase activation, a response reversed by*

283   *Fpr2/3 agonist treatment*

284   Microglial ROS production via the enzyme NADPH oxidase, also termed NOX2, is a key

285   response to inflammatory stimuli, primarily serving as an antimicrobial defence mechanism

286   [31]. There is evidence for activation of this enzyme in AD [32], hence we investigated whether

287   this was also the cellular source of ROS in our model. ROS production induced by stimulation

288   with 100 nM oAβ was sensitive to inclusion of two different NADPH oxidase inhibitors, 1 μM

289   diphenylene iodonium and 1 μg/ml apocynin (Figure 2A-B), strongly suggesting the

290   involvement of this enzyme. NADPH oxidase is not the only potential cellular source of ROS

291   however, with mitochondrial superoxide production playing a significant part in many

292   physiological and pathological processes [33]. However, examination of BV2 cells stimulated

293   with 100 nM oAβ found no change in mitochondrial superoxide production over 1 hr

294   (Supplemental Figure 2A), whereas exposure to the mitochondrial complex I inhibitor rotenone

295   (1 μM) resulted in a clear increase mitochondrial superoxide production compared to untreated

296   (Supplemental Figure 2A-2B).

297

298   Having previously showing that BV2 cells express murine Fpr2/3 [28], we investigated whether

299   activation of this receptor could reverse oAβ-induced ROS production. Treatment of cells with

300   the Fpr2/3 specific agonist QC1 (100nM), delivered 10 min after oAβ-stimulation restored ROS

301   production to baseline levels (Figure 2C-2D). Moreover, this effect was sensitive to pre-

302   treatment with the Fpr2/3 specific antagonist WRW$_4$ at 10 μM (Figure 2E). Notably, production

303   of ROS in response to oAβ itself was not affected by WRW$_4$ inclusion, indicating that oAβ is

304   not in this case signalling through Fpr2/3 (Figure 2E). Confirming these data, measurement of

305   total cellular H$_2$O$_2$ revealed that whilst this species was undetectable in unstimulated cells,

306   oAβ treatment caused significant production, an effect reversed by treatment with QC1 (Figure

307   2F).

308

309   NADPH oxidase is a multi-subunit enzyme, with its activation requiring the translocation of a

310   p67 subunit from the cytosol to associate with the plasma membrane-bound gp91 subunit [32].

311   Confocal microscopic analysis of BV2 cells stimulated with 100 nM oAβ indicated a clear

312   appearance of co-localised p67phox and gp91phox signal at the plasma membrane of the

313   cells, an effect that was again prevented by subsequent treatment (10 min post-oAβ) with 100

314   nM QC1 (Figure 2G).

315

316   *Fpr2/3 stimulation does not modify major cellular antioxidant systems*

317   Whilst we have shown the Fpr2/3 agonist QC1 to reverse oAβ-induced NADPH oxidase

318   activation and ROS production, it is plausible that this could also be achieved through

319   activation of intracellular antioxidant systems. However, neither the ratio of reduced to

320   oxidised glutathione, nor expression of the antioxidant enzymes haem oxygenase-1 or

321   superoxide dismutase-2 were affected by either treatment with 100nM oAβ, 100nM QC1 or a

322   combination of the two (Figure 3). These data suggest that the ROS production-suppressing

323   actions of Fpr2/3 activation occur through modulation at source rather than stimulation of

324   defensive systems.

325

326   *Promotion of the pentose phosphate pathway by oAβ is reversed by Fpr2/3 stimulation*

327   An important aspect of immune cell activation is a change in their preferred source of

328   metabolic energy, with inflammatory cells tending to favour glycolysis over mitochondrial

329   oxidative phosphorylation as their primary energy source [34]. We therefore investigated how

330   oAβ treatment of BV2 cells would affect their metabolism through use of the Agilent Seahorse

331   XF Analyser. Stimulation of BV2 cells with 100 nM oAβ significantly supressed basal

332   respiration without affecting either maximal respiration or spare respiratory capacity, an effect

333   reversed by treatment with 100 nM QC1 1 hr post-oAβ challenge (Figure 4A-E). This change

334   in respiration resulted in a decrease in ATP production from both oxidative phosphorylation

335   (Figure 4F) and glycolysis (Figure 4G) upon oAβ stimulation, an action again reversed by

336   Fpr2/3 activation with QC1 (Figure 4F-4G).

337

338   Production of ROS from NADPH oxidase is ultimately dependent, as its name suggests, upon

339   a constant source of intracellular NADPH [32]. The major source of NADPH production in the

340   cell is the pentose phosphate pathway, which siphons glucose-6-phosphate from glycolysis

341   into the production of 6-phosphogluconate and then ribose-5-phosphate, generating NADPH

342   in both steps [35]. As both glycolytic and mitochondrial respiratory rates were suppressed by

343   oAβ, we investigated whether pentose phosphate pathway activity had concomitantly risen

344   through measurement of the activity of the rate limiting enzyme for this pathway, glucose-6-

345   phosphate dehydrogenase (G6PD). Treatment of BV2 cells with 100 nM oAβ for 24 hrs caused

346   a significant increase in G6PD activity, an effect that was reversed to baseline upon

347   subsequent treatment with 100nM QC1 (Figure 4H, confirming the importance of this pentose

348   phosphate pathway shunt in the response to oAβ.

349

350   *oAβ stimulated ROS production is responsible for microglial-mediated neuronal toxicity and*

351   *can be reversed by Fpr2/3 activation*

352   Production of ROS by immune cells is primarily for the purpose of killing invading pathogens.

353   In the context of AD however, where no infectious agent has been discovered, production of

354   ROS may well damage bystander neurones, contributing to neurodegeneration. To investigate

355   the relationship between oAβ-triggered microglial ROS production and neuronal health, we

356   employed an *in vitro* co-culture model using BV2 cells and trans-retinoic acid-differentiated

357   SH-SY5Y cells. Initial experiments revealed that 100 nM oAβ showed no direct toxicity to

358   differentiated SH-SY5Y cells even after exposure for 24 hrs (Figure 5A). However,

359   administration of oAβ to co-cultures significantly and selectively enhanced apoptosis of SH-

360   SY5Y cells (Figure 5B-C) without affecting BV2 cell survival (Figure 5C), an effect that was

361   notably prevented by treatment with 100 nM QC1 1 hr after oAβ exposure. Notably,

362   differentiated SH-SY5Y cells did not express Fpr2/3 (Supplemental Figure 3). Confirming that

363   either direct contact or short-lived secretory factors were responsible for BV2 cell-mediated

364   toxicity, apoptosis of SH-SY5Y cells was not induced following treatment with conditioned

365   medium from oAβ-stimulated BV2 cultures (Figure 5D). Finally, to test whether BV2 cell ROS

366   production was the mediating agent for SH-SY5Y cytotoxicity, the experiment was repeated

367   in the presence of the antioxidant molecule α-tocopherol (10 μM). Inclusion of this antioxidant

368   prevented SH-SY5Y apoptosis in co-cultures treated with oAβ, indicating a direct mediatory

369   role of microglial ROS production.

370

371   **Discussion**

372

373   Despite over 300 clinical trials having been performed targeting either of the proposed toxic

374   mediators in AD, Aβ and hyperphosphorylated tau, we do not as yet have any successful

375   therapeutic approaches for the disease. This suggests that, at the least, these two proteins

376   cannot be the sole factors driving the disease [36]. Increasingly, the role of neuroinflammation

377   and the behaviour of microglia in AD has come under investigation [3,37], an approach given

378   further impetus by reports that ablation of microglia can halt brain atrophy in murine models

379   of Aβ-driven disease [38] and tauopathy [39]. Microglial activation can be both beneficial and

380   damaging, hence strategies that can control excessive inflammatory activity and promote a

381   pro-resolving phenotype may be of great potential for therapeutic use. In this study, we have

382   used an *in vitro* cellular model to provide proof-of-principle evidence for the targeting of the

383   pro-resolving receptor Fpr2/3 as a mechanism to restrain microglial behaviour and limit the

384   ability of these cells to damage bystander neurones.

385

386 Here, we report that alongside its well-characterised function in resolving inflammation and
387 efferocytosis [40], Fpr2/3 activation can reverse oAβ-induced ROS production through
388 deactivation of NADPH oxidase activity. Activation of microglial NADPH oxidase by oAβ is well
389 supported [41,42], and may be critical in triggering neuroinflammation, given the damaging
390 effects of oxidative stress for neurones, as has been reported in traumatic brain injury [43].
391 Future work will determine whether the *in vitro* findings we report here can be extended to the
392 *in vivo* situation, but if so, they suggest that the use of Fpr2/3 agonists capable of reversing
393 NADPH oxidase activation may be of therapeutic potential for AD.

394

395 The effects of Fpr2/3 activation upon oAβ-induced ROS production are mirrored by changes
396 in microglial metabolic phenotype. The importance of cellular metabolism in regulating
397 immune cell phenotype has become increasingly evident over the past few years, with a shift
398 from mitochondrial respiration to a glycolysis-dominant metabolism being closely associated
399 with a pro-inflammatory phenotype [34]. Metabolic changes in AD are well supported [44], but
400 the relationship between these changes and disease pathology is unclear. In the current study,
401 exposure of microglia to oAβ suppressed mitochondrial respiration, but rather than being
402 accompanied by changes to glycolysis, it was associated with a significant diversion of
403 glucose to the pentose phosphate pathway. Presumably, this was due to increased NADPH
404 demand associated with NADPH oxidase-driven ROS production, as seen in peripheral
405 macrophages [45]. Notably, Fpr2/3 agonist treatment was able to reverse the effects of oAβ
406 on microglial metabolism, targeting both the pentose phosphate pathway and the
407 mitochondria. This data adds to the increasing evidence suggesting that Fpr2/3 not only
408 suppresses pro-inflammatory mediator production [16,46], but aids in the regulation of the
409 underlying metabolic changes that occur in activated immune cells, as we have recently
410 shown in peripheral macrophages [14]. Importantly, microglia rapidly upregulate Fpr2/3
411 expression following inflammatory insult [47], and whilst the effects of its stimulation on
412 neuroinflammation can be agonist dependent [48], selective Fpr2/3 activation contributes to
413 neuroinflammatory resolution in a murine model of AD [46].

414

415 However, a notable finding of the current work is that we were unable to detect evidence for
416 an oAβ-induced microglial inflammatory response, in contrast to previous *in vitro* studies
417 [24,47,51]. This does not appear to be due to deficiency in the BV2 cells themselves, as
418 stimulation with bacterial lipopolysaccharide was still able to trigger a potent inflammatory
419 response. Notably, studies that report pro-inflammatory effects of oAβ have commonly used
420 micromolar concentrations of the peptide, several orders of magnitude greater than levels
421 reported to occur in the human brain in AD [30]. This suggests that the direct pro-inflammatory
422 effects of oAβ seen in *in vitro* may not be fully recapitulated *in vivo*, although this requires

423 further validation. Nevertheless, oAβ was clearly able to induce ROS production at levels
424 capable of damaging bystander cells, which if replicated *in vivo* may be a driving factor in
425 ongoing neuronal damage and secondary neuroinflammation seen in AD. Production of ROS
426 is far from the sole damaging effect of oAβ in the brain, as is borne out by the, at best,
427 equivocal results from clinical trials of antioxidants in AD [50,51]. Nevertheless, targeting a
428 receptor with the potential to suppress ROS production, restore microglial metabolic
429 homeostasis and promote resolution, as is the case for Fpr2/3, has significant potential for
430 therapeutic development.

431

432 The goal of this study was to provide proof-of-principle evidence that exploitation of human
433 FPR2 may hold promise as a therapeutic target for AD research. Evidently there are limitations
434 in how far the current study should be interpreted, with a particular need for further *in vivo*
435 validation of our findings. Nonetheless, the data presented do suggest that this receptor would
436 be a suitable target for anti-oxidative and metabolic therapeutic development for further AD
437 research, particularly as the effects of Fpr2/3 stimulation were apparent when stimulation
438 occurred after oAβ treatment. This study therefore adds novel insights into the role of Fpr2/3
439 in modulating microglial oxidative stress and metabolism, holding promise for select Fpr2/3
440 agonists as potent and effective treatment options for inflammatory disease [9].

441

442 **Conclusions**
443 This study has identified that although pathologically relevant concentrations of oAβ do not
444 appear to directly stimulate an inflammatory microglial phenotype, they are potent activators
445 of microglial ROS production via NADPH oxidase, and consequent changes to metabolic
446 phenotype. Moreover, activation of the pro-resolving receptor Fpr2/3 was able to reverse
447 these oAβ-induced changes and protect bystander neurones from damage. These data
448 suggest that manipulation of Fpr2/3 may be an important target for future therapeutic
449 development in neuroinflammatory conditions such as Alzheimer's disease.

450

451 **List of abbreviations**

452

453 AD: Alzheimer's disease
454 FPR2: Human formyl peptide receptor 2
455 Fpr2/3: Murine formyl peptide receptors 2/3
456 GSH: Reduced glutathione
457 GSSG: Oxidised glutathione
458 oAβ: Oligomeric β-amyloid 1-42
459 ROS: Reactive oxygen species

460   TNFα: Tumour necrosis factor alpha

461   WRW$_4$: Trp-Arg-Trp-Trp-Trp-Trp

462

463   **References**

464

465   1. United Nations. World Population Prospects: The 2015 Revision, Key Findings and

466   Advance Tables. World Popul. Prospect. 2015.

467   2. Prince MJ, Wimo A, Guerchet MMM, Gemma-Claire A, Wu Y-T, Prina M, et al. World

468   Alzheimer Report 2015 - The Global Impact of Dementia: An analysis of prevalence,

469   incidence, cost and trends. Alzheimer's Dis. Int. Alzheimer's Disease International; 2015.

470   3. Heneka MT, Carson MJ, Khoury J El, Landreth GE, Brosseron F, Feinstein DL, et al.

471   Neuroinflammation in Alzheimer's disease. Lancet Neurol. 2015;14:388–405.

472   4. Ransohoff RM, El Khoury J. Microglia in Health and Disease. Cold Spring Harb. Perspect.

473   Cold Spring Harbor Laboratory Press; 2015;8:a020560.

474   5. Taipa R, Ferreira V, Brochado P, Robinson A, Reis I, Marques F, et al. Inflammatory

475   pathology markers (activated microglia and reactive astrocytes) in early and late onset

476   Alzheimer disease: a *post mortem* study. Neuropathol. Appl. Neurobiol. 2018;44:298–313.

477   6. Spangenberg EE, Green KN. Inflammation in Alzheimer's disease: Lessons learned from

478   microglia-depletion models. Brain. Behav. Immun. 2017;61:1–11.

479   7. Heneka MT, Kummer MP, Latz E. Innate immune activation in neurodegenerative

480   disease. Nat. Publ. Gr. 2014;14.

481   8. Yu Y, Ye RD. Microglial Aβ Receptors in Alzheimer's Disease. Cell. Mol. Neurobiol.

482   2014;35:71–83.

483   9. Sugimoto MA, Vago JP, Perretti M, Teixeira MM. Mediators of the Resolution of the

484   Inflammatory Response. Trends Immunol. Elsevier Ltd; 2019;40:212–27.

485   10. Dufton N, Hannon R, Brancaleone V, Dalli J, Patel HB, Gray M, et al. Anti-inflammatory

486   role of the murine formyl-peptide receptor 2: ligand-specific effects on leukocyte responses

487   and experimental inflammation. J. Immunol. 2010;184:2611–9.

488   11. Solito E, Kamal A, Russo-Marie F, Buckingham JC, Marullo S, Perretti M. A novel

489   calcium-dependent proapoptotic effect of annexin 1 on human neutrophils. FASEB J.

490   2003;17:1544–6.

491   12. Drechsler M, de Jong R, Rossaint J, Viola JR, Leoni G, Wang JM, et al. Annexin A1

492   counteracts chemokine-induced arterial myeloid cell recruitment. Circ. Res. 2015;116:827–

493   35.

494   13. McArthur S, Gobbetti T, Kusters DHM, Reutelingsperger CP, Flower RJ, Perretti M.

495   Definition of a Novel Pathway Centered on Lysophosphatidic Acid To Recruit Monocytes

496   during the Resolution Phase of Tissue Inflammation. J. Immunol. 2015;195:1500733.

497   14. McArthur S, Juban G, Gobbetti T, Desgeorges T, Theret M, Gondin J, et al. Annexin A1

498   drives macrophage skewing to accelerate muscle regeneration through AMPK activation. J.

499   Clin. Invest. 2020;124635.

500   15. Scannell M, Flanagan MB, deStefani A, Wynne KJ, Cagney G, Godson C, et al.

501   Annexin-1 and peptide derivatives are released by apoptotic cells and stimulate

502   phagocytosis of apoptotic neutrophils by macrophages. J. Immunol. 2007;178:4595–605.

503   16. Gobbetti T, Coldewey SMSM, Chen J, McArthur S, le Faouder P, Cenac N, et al.

504   Nonredundant protective properties of FPR2/ALX in polymicrobial murine sepsis. Proc. Natl.

505   Acad. Sci. U. S. A. 2014;111:18685–90.

506   17. Kain V, Jadapalli JK, Tourki B, Halade G V. Inhibition of FPR2 impaired leukocytes

507   recruitment and elicited non-resolving inflammation in acute heart failure. Pharmacol. Res.

508   2019;146:104295.

509   18. Petri MH, Laguna-Fernandez A, Arnardottir H, Wheelock CE, Perretti M, Hansson GK, et

510   al. Aspirin-triggered lipoxin A4 inhibits atherosclerosis progression in apolipoprotein E $^{-/-}$

511   mice. Br. J. Pharmacol. 2017;

512   19. Ho CF-Y, Ismail NB, Koh JK-Z, Gunaseelan S, Low Y-H, Ng Y-K, et al. Localisation of

513   Formyl-Peptide Receptor 2 in the Rat Central Nervous System and Its Role in Axonal and

514   Dendritic Outgrowth. Neurochem. Res. 2018;43:1587–98.

515   20. Iribarren P, Zhou Y, Hu J, Le Y, Wang JM. Role of formyl peptide receptor-like 1

516   (FPRL1/FPR2) in mononuclear phagocyte responses in Alzheimer disease. Immunol. Res.

517   2005;31:165–76.

518   21. Cui YH, Le Y, Zhang X, Gong W, Abe K, Sun R, et al. Up-regulation of FPR2, a

519   chemotactic receptor for amyloid beta 1-42 (A beta 42), in murine microglial cells by TNF

520   alpha. Neurobiol. Dis. 2002;10:366–77.

521   22. Le Y, Gong W, Tiffany HL, Tumanov A, Nedospasov S, Shen W, et al. Amyloid (beta)42

522   activates a G-protein-coupled chemoattractant receptor, FPR-like-1. J. Neurosci.

523   2001;21:RC123.

524   23. Tiffany HL, Lavigne MC, Cui YH, Wang JM, Leto TL, Gao JL, et al. Amyloid-beta induces

525   chemotaxis and oxidant stress by acting at formylpeptide receptor 2, a G protein-coupled

526   receptor expressed in phagocytes and brain. J. Biol. Chem. American Society for

527   Biochemistry and Molecular Biology; 2001;276:23645–52.

528   24. Ries M, Loiola R, Shah UN, Gentleman SM, Solito E, Sastre M. The anti-inflammatory

529   Annexin A1 induces the clearance and degradation of the amyloid-β peptide. J.

530   Neuroinflammation. 2016;13:234.

531   25. Stine B, Jungbauer L, Chunjiang Y, LaDu M. Preparing Synthetic Aβ in Different

532   Aggregation States. Methods Mol. Biol. 2011;670:13–32.

533   26. Shipley MM, Mangold CA, Szpara ML. Differentiation of the SH-SY5Y Human

534   Neuroblastoma Cell Line. J. Vis. Exp. MyJoVE Corporation; 2016;53193.

535   27. Mookerjee SA, Gerencser AA, Nicholls DG, Brand MD. Quantifying intracellular rates of

536   glycolytic and oxidative ATP production and consumption using extracellular flux

537   measurements. J. Biol. Chem. American Society for Biochemistry and Molecular Biology;

538   2017;292:7189–207.

539   28. McArthur S, Cristante E, Paterno M, Christian H, Roncaroli F, Gillies GEE, et al. Annexin

540   A1: a central player in the anti-inflammatory and neuroprotective role of microglia. J

541   Immunol. 2010/10/22. 2010;185:6317–28.

542   29. Loiola RA, Wickstead ES, Solito E, McArthur S. Estrogen promotes pro-resolving

543   microglial behaviour and phagocytic cell clearance through the actions of annexin A1. Front.

544   Endocrinol. (Lausanne). Cold Spring Harbor Laboratory; 2019;10:420.

545   30. Helmond Z Van, Miners JS, Kehoe PG, Love S. Higher Soluble Amyloid b Concentration

546   in Frontal Cortex of Young Adults than in Normal Elderly or Alzheimer ' s Disease.

547   2010;20:787–93.

548   31. Spooner R, Yilmaz O. The role of reactive-oxygen-species in microbial persistence and

549   inflammation. Int. J. Mol. Sci. Multidisciplinary Digital Publishing Institute (MDPI);

550   2011;12:334–52.

551   32. Ma MW, Wang J, Zhang Q, Wang R, Dhandapani KM, Vadlamudi RK, et al. NADPH

552   oxidase in brain injury and neurodegenerative disorders. Mol. Neurodegener. 2017;12:7.

553   33. Zorov DB, Juhaszova M, Sollott SJ. Mitochondrial reactive oxygen species (ROS) and

554   ROS-induced ROS release. Physiol. Rev. American Physiological Society; 2014;94:909–50.

555   34. O'Neill LAJ, Kishton RJ, Rathmell J. A guide to immunometabolism for immunologists.

556   Nat. Rev. Immunol. 2016;16:553–65.

557   35. Grant CM. Metabolic reconfiguration is a regulated response to oxidative stress. J. Biol.

558   BioMed Central; 2008. p. 1.

559   36. Makin S. The amyloid hypothesis on trial. Nature. 2018;559:S4–7.

560   37. Merlini M, Rafalski VA, Rios Coronado PE, Gill TM, Ellisman M, Muthukumar G, et al.

561   Fibrinogen Induces Microglia-Mediated Spine Elimination and Cognitive Impairment in an

562   Alzheimer's Disease Model. Neuron. 2019;101:1099-1108.e6.

563   38. Spangenberg EE, Lee RJ, Najafi ARR, Rice RAA, Elmore MRPRP, Blurton-Jones M, et

564   al. Eliminating microglia in Alzheimer's mice prevents neuronal loss without modulating

565   amyloid-β pathology. Brain. Oxford University Press; 2016;139:1265–81.

566   39. Shi Y, Manis M, Long J, Wang K, Sullivan PM, Remolina Serrano J, et al. Microglia drive

567   APOE-dependent neurodegeneration in a tauopathy mouse model. J. Exp. Med. Rockefeller

568   University Press; 2019;jem.20190980.

569   40. Corminboeuf O, Leroy X. FPR2/ALXR Agonists and the Resolution of Inflammation. J.

570   Med. Chem. 2015;58:537–59.

571   41. Abubaker AA, Vara D, Visconte C, Eggleston I, Torti M, Canobbio I, et al. Amyloid

572   Peptide β1-42 Induces Integrin αIIbβ3 Activation, Platelet Adhesion, and Thrombus

573   Formation in a NADPH Oxidase-Dependent Manner. Oxid. Med. Cell. Longev.

574   2019;2019:1050476.

575   42. Alawieyah Syed Mortadza S, Sim JA, Neubrand VE, Jiang L-H. A critical role of TRPM2

576   channel in Aβ42 -induced microglial activation and generation of tumor necrosis factor-α.

577   Glia. 2018;66:562–75.

578   43. Kumar A, Barrett JP, Alvarez-Croda D-M, Stoica BA, Faden AI, Loane DJ. NOX2 drives

579   M1-like microglial/macrophage activation and neurodegeneration following experimental

580   traumatic brain injury. Brain. Behav. Immun. 2016;58:291–309.

581   44. Mostafavi S, Gaiteri C, Sullivan SE, White CC, Tasaki S, Xu J, et al. A molecular network

582   of the aging human brain provides insights into the pathology and cognitive decline of

583   Alzheimer's disease. Nat. Neurosci. 2018;21:811–9.

584   45. Nagy C, Haschemi A. Time and Demand are Two Critical Dimensions of

585   Immunometabolism: The Process of Macrophage Activation and the Pentose Phosphate

586   Pathway. Front. Immunol. Frontiers; 2015;6:164.

587   46. Kantarci A, Aytan N, Palaska I, Stephens D, Crabtree L, Benincasa C, et al. Combined

588   administration of resolvin E1 and lipoxin A4 resolves inflammation in a murine model of

589   Alzheimer's disease. Exp. Neurol. 2018;300:111–20.

590   47. Chen K, Iribarren P, Huang J, Zhang L, Gong W, Cho EH, et al. Induction of the Formyl

591   Peptide Receptor 2 in Microglia by IFN- and Synergy with CD40 Ligand. J. Immunol.

592   2007;178:1759–66.

593   48. He H-Q, Ye R. The Formyl Peptide Receptors: Diversity of Ligands and Mechanism for

594   Recognition. Molecules. Multidisciplinary Digital Publishing Institute; 2017;22:455.

595   49. Liu H, Wang JJ, Wang JJ, Wang P, Xue Y. Paeoniflorin attenuates Aβ1-42-induced

596   inflammation and chemotaxis of microglia in vitro and inhibits NF-κB- and VEGF/Flt-1

597   signaling pathways. Brain Res. 2015;1618:149–58.

598   50. D'Cunha NM, Georgousopoulou EN, Dadigamuwage L, Kellett J, Panagiotakos DB,

599   Thomas J, et al. Effect of long-term nutraceutical and dietary supplement use on cognition in

600   the elderly: a 10-year systematic review of randomised controlled trials. Br. J. Nutr.

601   2018;119:280–98.

602   51. McCleery J, Abraham RP, Denton DA, Rutjes AW, Chong L-Y, Al-Assaf AS, et al.

603   Vitamin and mineral supplementation for preventing dementia or delaying cognitive decline

604   in people with mild cognitive impairment. Cochrane Database Syst. Rev.

605   2018;11:CD011905.

606

607

608   **Figure Legends**

609

610   **Figure 1: oAβ stimulates microglial ROS production without inducing an inflammatory**

611   **response. A)** Treatment with oAβ dose-dependently induces microglial ROS production rate

612   over a 2 hr period. **B)** Treatment of BV2 cells with 50 ng/ml LPS but not 100 nM oAβ increased

613   microglial TNFα production after 24 and 48 hrs exposure. **C)** Treatment for 24 hrs with 50

614   ng/ml LPS but not 100nM oAβ increased BV2 cell surface CD40 expression. **D)** Neither

615   treatment for 24 nor 48 hrs with 100nM oAβ affected phagocytosis by BV2 cells of heat-killed

616   E. coli bacterial particles. 50 ng/ml LPS increased phagocytosis at 48 hrs only. In all cases,

617   data are mean ± SEM of 3-6 independent cultures, assayed in triplicate. *p<0.05 *vs.* untreated

618   cells.

619

620   **Figure 2: oAβ induced ROS production follows activation of NADPH oxidase and is**

621   **reversed by subsequent Fpr2/3 stimulation. A, B)** oAβ induced ROS production was

622   prevented by 10 min pre-treatment with the NADPH oxidase inhibitors DPI (1 μM, A) and

623   apocynin (1 μg/ml, B). **C)** Representative time-course of ROS production in untreated BV2

624   cells, and cells exposed to 100nM oAβ with or without subsequent stimulation with 100nM

625   QC1 (10 min post-oAβ). **D)** Average ROS production rates for BV2 cells treated with oAβ (100

626   nM, 1 hr) with or without subsequent stimulation with 100 nM QC1 (10 min post-oAβ). **E)**

627   Inclusion of the selective Fpr2/3 antagonist WRW$_4$ (10μM, 10 min prior to oAβ treatment) did

628   not affect 100 nM oAβ-induced ROS production, but prevented the effects of subsequent

629   treatment with QC1 (100 nM, 10 min post-oAβ). **F)** Treatment of BV2 cells for 30 min with 100

630   nM oAβ stimulated co-localisation of the NADPH oxidase subunits p67phox (green) and

631   gp91phox (red), an effect prevented by treatment with 100 nM QC1 administered 10 min post-

632   oAβ. Nuclei are counter-stained with DAPI (blue); p67phox and gp91phox co-localisation

633   intensity is represented by the false-colour plots. Graphical data are mean ± SEM of 3-6

634   independent cultures, assayed in triplicate, *p<0.05. Images represent cells from 3

635   independent cultures; scale bar = 10 μm.

636

637   **Figure 3: Neither treatment with oAβ nor QC1 affected major cellular antioxidant**

638   **systems. A)** The ratio of reduced (GSH) to oxidised (GSSG) glutathione within BV2 cell

639   cytoplasm was not affected by either oAβ (100 nM, 2 hrs) or QC1 (100 nM, 10 min post-oAβ)

640   administration. **B)** Expression of the antioxidant enzyme haem oxygenase-1 (HO-1) was not

641   affected by treatment with oAβ (100 nM, 6 hrs) or QC1 (100 nM, 10 min post-oAβ). Sample

642   loading was normalised to Ponceau S-defined total protein content; densitometric analysis

643   data are mean ± SEM of 3 independent cultures. **C)** Expression of the antioxidant enzyme

644   superoxide dismutase-2 (SOD-2) was not affected by treatment with oAβ (100 nM, 24 hrs) or

645   QC1 (100nM, 10 min post-oAβ). All western blot analyses are representative of 3 independent

646   cultures, with sample loading normalised to Ponceau S-defined total protein content;

647   densitometric analysis data are mean ± SEM of 3 independent cultures, quantified in triplicate.

648

649   **Figure 4: Treatment with oAβ suppresses mitochondrial respiration and promotes**

650   **activity of the pentose phosphate pathway, effects reversed by subsequent activation**

651   **of Fpr2/3. A)** Typical oxygen consumption rates of untreated BV2 cells and cells treated for

652   24 hrs with 100 nM oAβ with or without subsequent stimulation with QC1 (100 nM, 1 hr post-

653   oAβ), administration times for oligomycin (4 µM), FCCP (0.6 µM) and rotenone with antimycin

654   A (both 1 µM) are indicated. **B)** Typical extracellular acidification rates for untreated BV2 cells

655   and cells treated for 24 hrs with 100 nM oAβ with or without subsequent stimulation with QC1

656   (100 nM, 1 hr post-oAβ), administration times for oligomycin (4 µM), FCCP (0.6 µM) and

657   rotenone with antimycin A (both 1 µM) are indicated. **C-E)** Treatment with 100 nM oAβ for 24

658   hrs significantly suppressed basal metabolic rate (C), an effect that no longer reached

659   statistical significance after QC1 treatment (100 nM, 1 hr post-oAβ). In contrast, neither oAβ

660   nor QC1 treatment affected maximal respiration (D) or spare respiratory capacity (E). **F)**

661   Treatment with oAβ (100 nM, 24 hrs) significantly suppressed basal, but not maximal, ATP

662   production due to mitochondrial oxidative phosphorylation, an effect reversed by subsequent

663   treatment with QC1 (100 nM, 1 hr post-oAβ). **G)** ATP generation from glycolysis was

664   unaffected by either oAβ or QC1 treatment. **H)** Activity of the rate-determining enzyme of the

665   pentose phosphate pathway, glucose-6-phosphate dehydrogenase (G6PD) was significantly

666   increased by treatment with 100nM oAβ (24 hrs), an effect reversed by subsequent stimulation

667   with 100 nM QC1 (1 hr post-oAβ). All data are mean ± SEM for 3-5 independent cultures,

668   assayed in triplicate, *p<0.05.

669

670   **Figure 5: Treatment with oAβ induces differentiated SH-SY5Y neuronal apoptosis only**

671   **in the presence of microglia, acting through Fpr2/3 sensitive ROS release. A)** Treatment

672   with oAβ (100 nM, 48 hrs) had no effect on *trans*-retinoic acid (tRA)-differentiated SH-SY5Y

673   cell viability; data are mean ± SEM of 5 independent cultures, assayed in triplicate. **B)**

674   Separation of tRA-differentiated SH-SY5Y neurons from BV2 cells grown in co-culture on the

675   basis of differential CD200 and CD11b expression, plot is representative of 3 independent

676   cultures. **C)** Treatment of co-cultures of BV2 and tRA-differentiated SH-SY5Y neurons with

677   oAβ (100 nM, 48 hrs) induces significant SH-SY5Y apoptosis, an effect prevented by

678   subsequent treatment with QC1 (100 nM, 10 min post-oAβ). **D)** Conditioned medium from BV2

679   cells treated or not with 100nM oAβ (24 hrs) had no effect on tRA-differentiated SH-SY5Y

680   neuronal apoptosis following exposure for 48 hrs. **E)** Inclusion of the antioxidant α-tocopherol

681   (10 µM) in co-cultures of BV2 cells and tRA-differentiated SH-SY5Y neurons prevented oAβ-

682   induced (100 nM, 48 hrs) neuronal apoptosis; data are mean ± SEM for 3-6 independent

683   cultures, assayed in triplicate, *p<0.05.

684

685   **Supplemental Figure 1: Approximate molecular weight of Aβ1-42 oligomers following**

686   **polyacrylamide gel electrophoresis under non-denaturing conditions.** As monomeric

687      $Aβ_{1-42}$ has a molecular weight of 4.51 kDa, the apparent molecular weight of approximately

688   35kDa suggest that oAβ species were hexamers/heptamers.

689

690   **Supplementary Figure 2: Mitochondrial ROS production is not stimulated in microglia**

691   **by oAβ treatment. A)** Representative time-course of mitochondrial superoxide production in

692   untreated BV2 cells and cells exposed to 100 nM oAβ, 100nM QC1 or 1 µM rotenone for 1 hr.

693   **B)** Average mitochondrial superoxide production rates for untreated BV2 cells and cells

694   treated with oAβ (100 nM, 1 hr), QC1 (100 nM, 1 hr) or rotenone (ROT; 1 µM, 1 hr); data are

695   mean ± SEM of 4 independent cultures, assayed in triplicate, *p<0.05.

696

697   **Supplementary Figure 3: FPR2 is not expressed by SH-SY5Y cells. A)** representative

698   forward scatter-side scatter histogram plot and gating strategy. **B)** representative histogram

699   plot to exclude cell doublets. **C**) histogram of relative FPR2 staining. Neither naïve or trans-

700   retinoic acid induced differentiated SH-SY5Y cells expressed FPR2.

701

Figure 1: oAβ stimulates microglial ROS production, but does not induce an inflammatory response

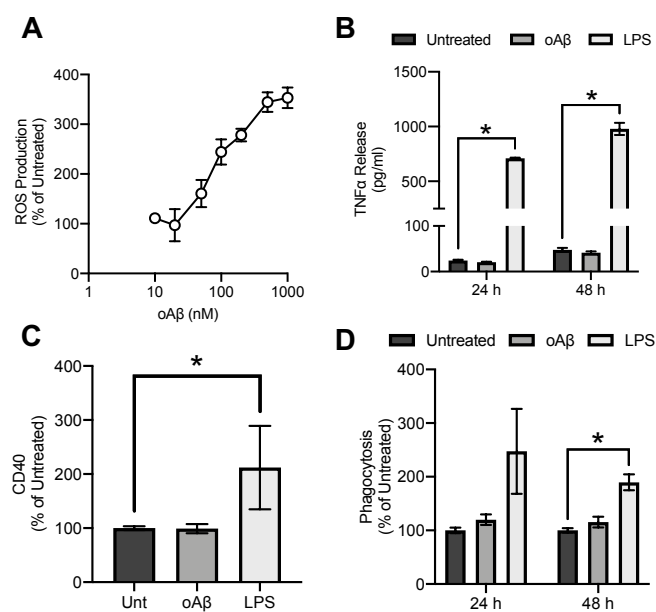Figure 2: oAβ induced ROS production follows activation of NADPH oxidase, and can be reversed by subsequent stimulation with the Fpr2 agonist QC1
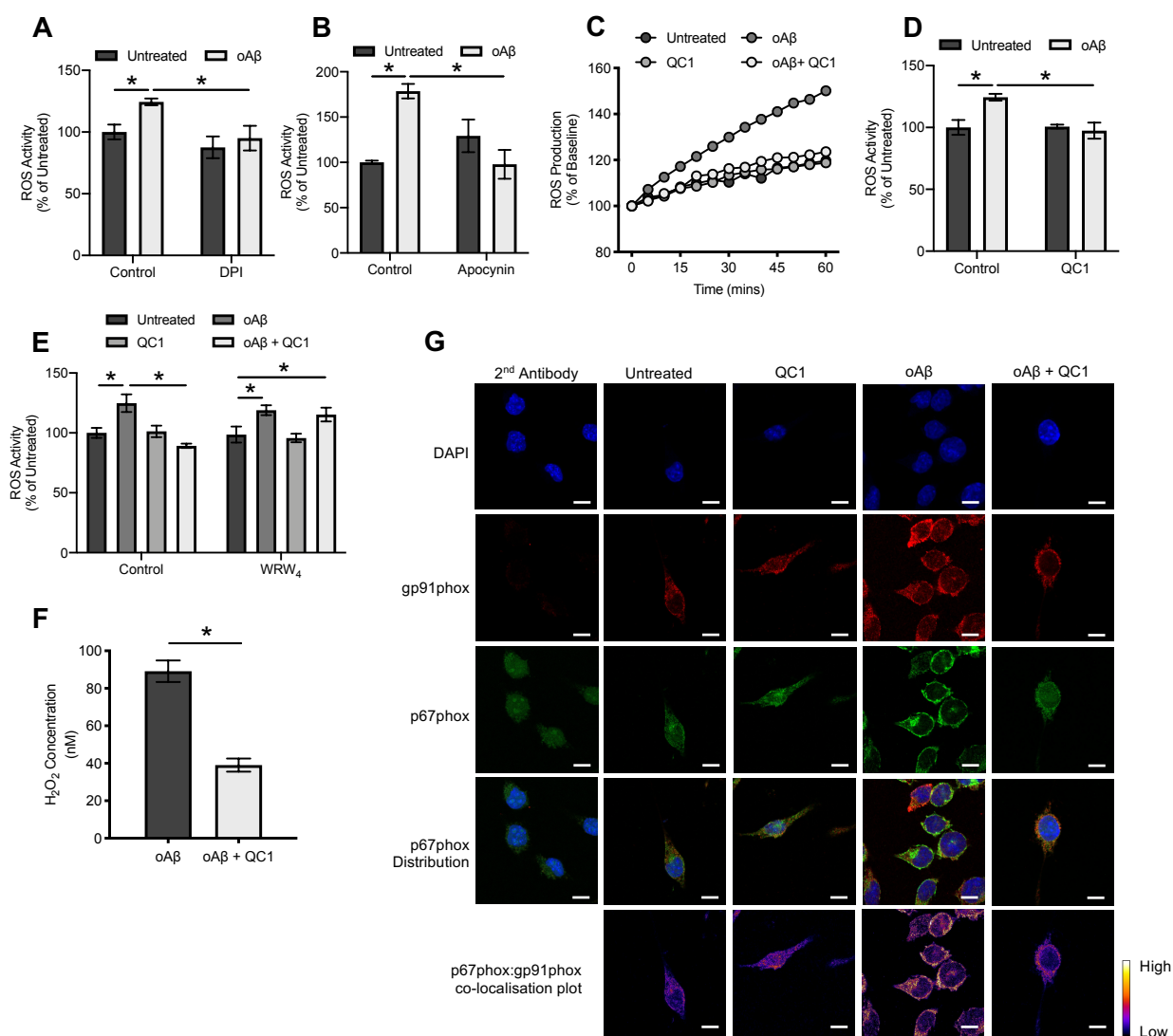
Figure 3: Neither treatment with oAβ nor QC1 affected the major cellular antioxidant systems, glutathione, haem oxygenase-1 or superoxide dismutase-2
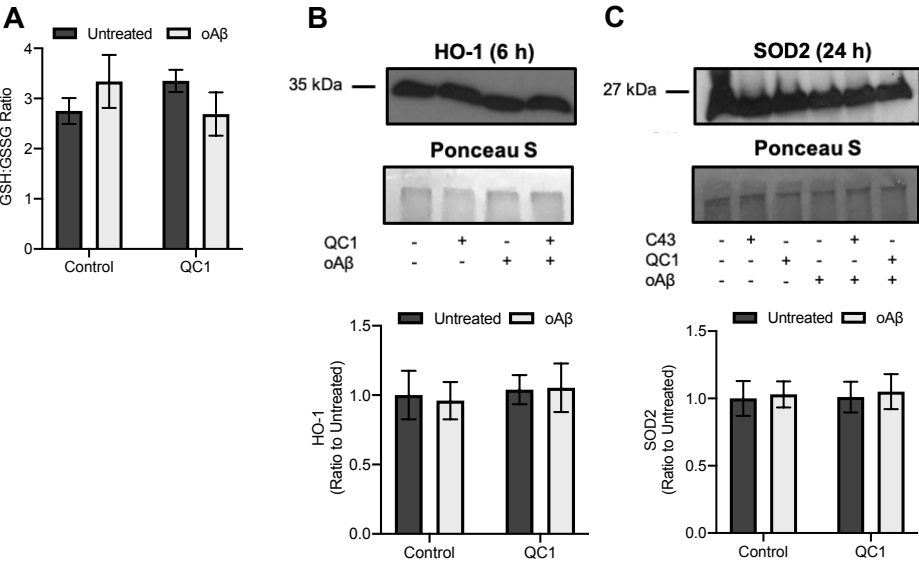
Figure 4: Treatment with oAβ suppresses mitochondrial respiration and promotes activity of the pentose phosphate pathway, effects reversed by subsequent activation of Fpr2/3
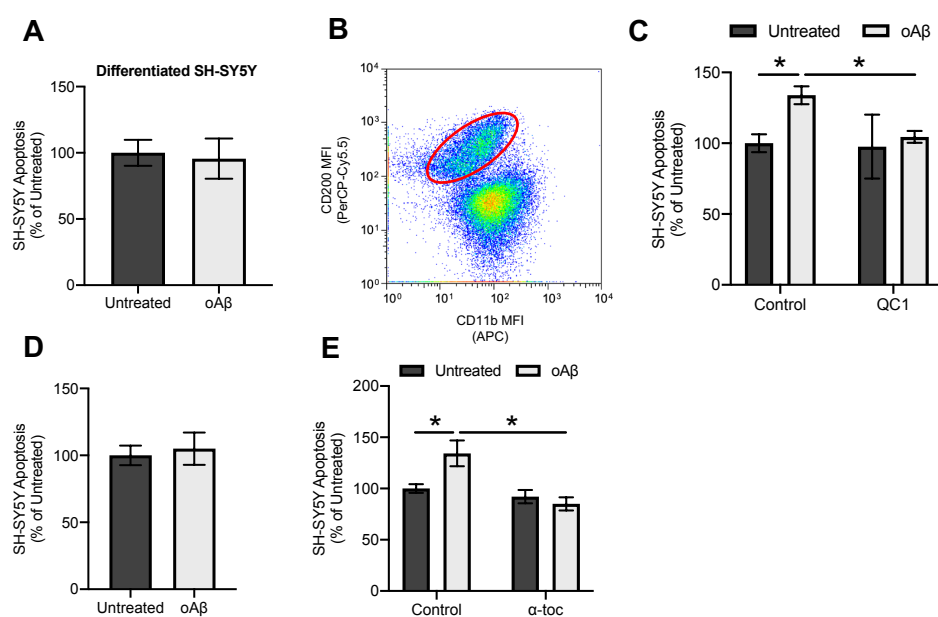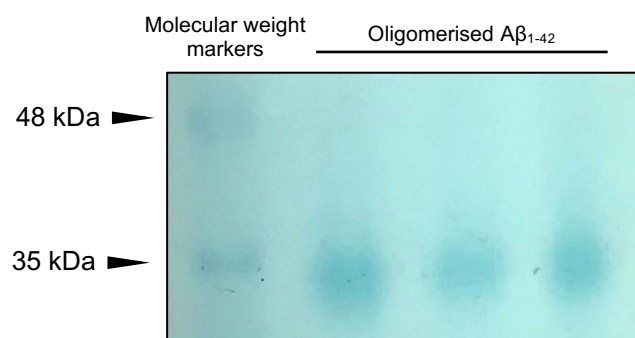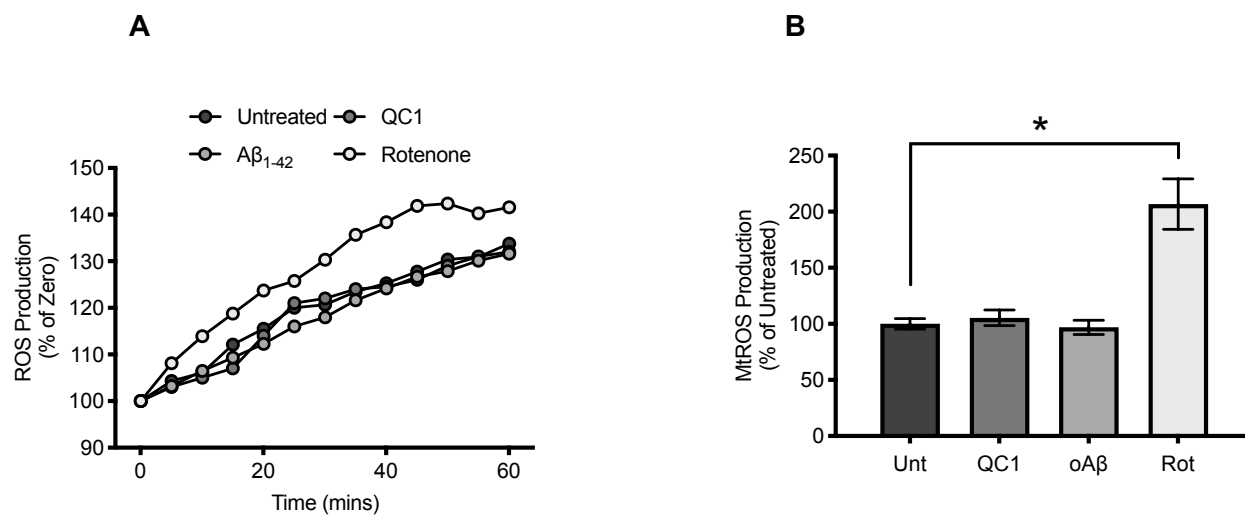
Figure 5: Treatment with oAβ increases SH-SY5Y apoptosis in BV-2 co-culture through microglial induced ROS production.

Supplementary Figure 1: Oligomerisation of Aβ$_{1-42}$ produces hexamers/heptamers

Supplementary Figure 2: Mitochondrial ROS production does not appear to be stimulated by oAβ treatment

Supplementary Figure 3: FPR2 is not expressed in SH-SY5Y cells